Plane Spiral OAM Mode-Group Orthogonal Multiplexing Communication Using Partial Arc Sampling Receiving Scheme

Xiaowen Xiong, *Member, IEEE*, Shilie Zheng, *Member, IEEE*, Yuqi Chen, *Graduate Student Member, IEEE*, Zelin Zhu, *Graduate Student Member, IEEE*, Xiaonan Hui, *Member, IEEE*, Xianbin Yu, *Senior Member, IEEE*, Xiaofeng Jin, *Member, IEEE*, Wei E. I. Sha, *Senior Member, IEEE*, and Xianmin Zhang, *Member, IEEE*

***Abstract*— A variety of novel orbital angular momentum (OAM)-based communication or sensing systems have attracted much attention over the past decade, the superiority is brought about by nothing other than its orthogonality or vorticity. Plane spiral OAM (PSOAM) mode-group (MG) technique as a reconfigurable beamforming method can be used for building a multiple-in-multiple-out (MIMO) system to achieve the reduction in subchannel correlation, which benefits from the spiral phase distribution within the mainlobe. However, the demultiplexing process still depends on the MIMO algorithm, in which the receiver complexity is same as the conventional MIMO systems. In this article, a PSOAM MG orthogonal multiplexing communication link at the X-band using partial arc sampling receiving (PASR) scheme has been demonstrated experimentally. The MG channels have a good isolation of about 15 dB, and the existing performance can ensure the reliable 16-QAM wireless transmission. Besides, a real-time dual-channel video transmission experiment has been carried out to verify the channel isolation caused by MG's orthogonality intuitively. More importantly, the demultiplexing procedure using the PASR scheme can be implemented by simple analog phase shifting operation with a lower receiver complexity compared with the conventional MIMO systems.**

***Index Terms*— Mode-group (MG), orbital angular momentum (OAM), orthogonality, partial arc sampling receiving (PASR), wireless communication.**

Manuscript received 10 November 2021; revised 9 May 2022; accepted 22 June 2022. Date of publication 12 July 2022; date of current version 17 November 2022. This work was supported in part by the National Key Research and Development Program of China under Grant 2018YFB2201700; in part by the National Natural Science Foundation of China under Grant 62171409, Grant 61571391, Grant 61975177, and Grant U20A20164; and in part by the Zhejiang Laboratory under Grant 2020LC0AD01. *(Corresponding authors: Shilie Zheng; Xianmin Zhang.)*

Xiaowen Xiong, Shilie Zheng, Yuqi Chen, Zelin Zhu, Xiaofeng Jin, and Wei E. I. Sha are with the College of Information Science and Electronic Engineering, Zhejiang University, Hangzhou 310027, China (e-mail: zhengsl@zju.edu.cn).

Xiaonan Hui and Xianbin Yu are with the College of Information Science and Electronic Engineering, Zhejiang University, Hangzhou 310027, China, and also with the Zhejiang Laboratory, Hangzhou 311121, China.

Xianmin Zhang is with the College of Information Science and Electronic Engineering, Zhejiang University, Hangzhou 310027, China, and also with the School of Information Science and Engineering, NingboTech University, Ningbo 315100, China (e-mail: zhangxm@zju.edu.cn).

Color versions of one or more figures in this article are available at https://doi.org/10.1109/TAP.2022.3188386.

Digital Object Identifier 10.1109/TAP.2022.3188386

I. Introduction

THANKS to the phase diversity and the spatial orthogonality, orbital angular momentum (OAM) has caught worldwide researchers' interests in the fields of high-speed microwave [1], [2], THz [3] or optical [4] communication systems, radar detection/imaging [5], [6], physical layer security [7], [8], etc. OAM waves have the helical phase front of $e^{jl\varphi}$, where φ and l refer to the azimuthal angle and the OAM order, respectively [9]. Different from the spin angular momentum with only the finite multiplexing dimensions, theoretically, OAM has infinite orthogonal modes that are allowed to be multiplexed [10], which may increase the communication capacity manyfold [11].

Except for the idea of mode division multiplexing (MDM) [12], the superposition of several specific OAM waves has been verified to be an eigenmode beamforming method to realize the azimuthal pattern diversity [13], [16]. Such generated beam can be defined as OAM mode-group (MG) [15]. However, owing to the center phase singularity and inconsistency of beam divergence [16]–[19], it is quite hard for the conventional OAM wave to overlap their mainlobes in free space, and hence, it is difficult to realize eigenmode beamforming. Zheng *et al.* [13] proposed a special form of OAM wave called *plane spiral OAM* (PSOAM) wave. Compared with the conventional OAM wave propagating along the z-direction, PSOAM wave can be known as a 2-D structure which propagates along the transverse plane with azimuthal spiral phase distribution. Different PSOAM waves have consistent divergence angles θ_d of 90°, i.e., they can propagate along the same propagation directions [20]. Meanwhile, the phase singularity is inside the PSOAM antenna, and the energy hole will be avoided reasonably along the propagation path. Thanks to these characteristics, PSOAM waves are more suitable for realizing the above-mentioned eigenmode beamforming in practice. Certainly, PSOAM MG can be regarded as a special kind of OAM MG.

A PSOAM MG possesses two prime features: the *directionality* brought about by beamforming effect and the *vorticity* similar to the single-mode OAM wave [13], i.e., it presents a high-gain beam with spiral phase distribution

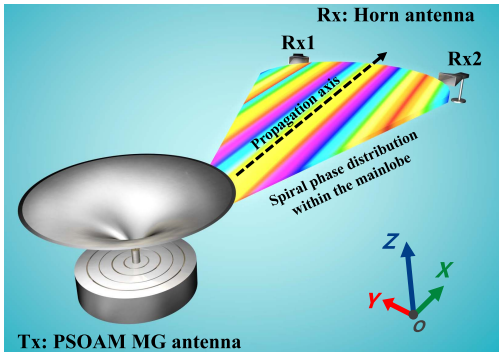

Fig. 1. PSOAM MG multiplexing communication system. To use the PASR scheme, the MGs need to be radiated coaxially; besides, the receiving antennas also need to be placed symmetrically along the propagation axis.

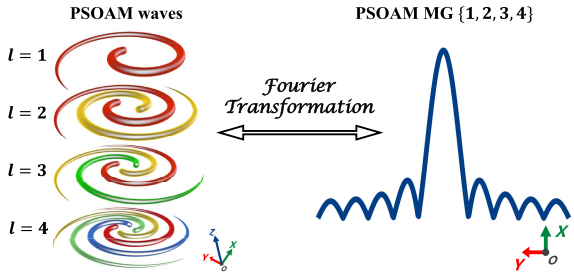

Fig. 2. Azimuthal angle and PSOAM modes can be connected by *Fourier transformation*.

within its mainlobe in the azimuthal direction and also propagates along the transverse plane. In [21], a PSOAM-MG-based multiple-in-multiple-out (MIMO) system (MG-MIMO) has been demonstrated experimentally. It has been proven that MG's directionality can improve the signal-to-noise ratio (SNR) level and its vorticity can introduce the additional phase shift to further decrease the spatial correlation. Besides, the MG-MIMO system shows better robustness than the existing MIMO system. However, MG's orthogonality is not used for realizing the demultiplexing process, and the MG-MIMO system still needs to rely on common MIMO algorithm to separate the multiplexed data streams. From the perspective of receiver complexity, the MG-MIMO system has no superiorities. Previously, the partial arc sampling receiving (PASR) scheme [22] has been proposed to demultiplex several single-mode OAM waves orthogonally in a limited, smaller, and reasonable aperture, which can overcome the difficulty of receiving the beams with the whole angular aperture in a long-distance transmission scenario. Thanks to its mainlobe's spiral phase distribution similar to the conventional OAM wave, PSOAM MG also possesses the orthogonality under the PASR scheme, which means that such PASR scheme can also be used for demultiplexing the data streams orthogonally in an MG multiplexing link. Remarkably, the demultiplexing process can be completely realized by simple analog phase shifting operation, and the receiver complexity will be reduced significantly. Hence, this article is different from [21]. The similarity between two works is that both adopt the PSOAM MG technology, but they take advantage of different properties of PSOAM MG. This work can be regarded as the extension, expansion, and development of previous work [21], which may provide the theoretical and practical basis for promoting the applications of MG technology in the communication system.

In this article, it is the first time to demonstrate a PSOAM MG orthogonal multiplexing communication link using the PASR scheme experimentally. Fig. 1 shows the sketch map of such the link. To demultiplex the MGs orthogonally, the transmitting end needs to adopt the coaxial arraying way. Moreover, the receiving antennas need to be placed at the symmetric positions along the propagation axis. It is worth noting that the demultiplexing procedure can be implemented by pure hardware with a lower complexity in this system. A compact PSOAM MG antenna [16] made up of coaxial resonators and a reflector are used for radiating the MGs. Furthermore, the significant experimental results including the isolation between multiplexed MGs and raw BER have also been evaluated in a realistic line-of-sight (LoS) scenario. Based on this communication architecture, a real-time dual-channel video multiplexing transmission experiment has been carried out finally.

II. MG Multiplexing Communication Using PASR Scheme

A. Orthogonality Under PASR Scheme

As shown in Fig. 2, owing to the same propagation direction, PSOAM waves can be considered as a suitable set of spatial eigenmodes to realize beamforming with azimuthal pattern diversity [13]. The azimuthal angle and PSOAM modes can form a set of *Fourier transformation* pairs [23]. Hence, for a MG^n $\{l_0^n, l_0^n + \Delta l, \ldots, l_0^n + (M-1)\Delta l\}$ superposed by M PSOAM modes l_0^n, $l_0^n + \Delta l$, …, $l_0^n + (M-1)\Delta l$, its theoretical pattern distribution in the azimuthal direction

$$F_{\mathrm{MG}^n}(\theta_0, \varphi) = \sum_{m=0}^{M-1} A_m(\theta_0) \cdot e^{j[(l_0^n + m\Delta l)\varphi + \varphi_0^m]} \tag{1}$$

where A_m refers to the intensity of the mth PSOAM wave among MG^n; Δl is the mode interval; l_0^n is the first PSOAM mode among MG^n; φ_0^m is the initial phase of the mth PSOAM wave; θ_0 denotes the propagation direction of single-mode PSOAM wave, and its value is equal to 90°. For the case of same amplitude (the values of A_m are all set as 1) and in-phase (the values of φ_0^m are all set as 0°), the pattern function (1) can be given ulteriorly by [21]

$$F_{\mathrm{MG}^n}(\varphi) \overset{\theta_0=90^\circ}{=} \frac{\sin(\frac{M\varphi}{2}\Delta l)}{\sin(\frac{\varphi}{2}\Delta l)} \cdot e^{j(l_0^n + \Delta l \frac{M-1}{2})\varphi} \tag{2}$$

From (2), it can be seen that the pattern function has been extended to the product of two parts: the former intensity term and the latter phase term. The former represents the directionality of MG^n in the azimuthal direction, and the latter characterizes the maiblobe's phase distribution of MG^n. With a certain strategy to select several successive PSOAM modes and superpose them into an MG, a high-gain pencil beam can be realized by manipulating the amplitude and the phase of each PSOAM mode among MG.

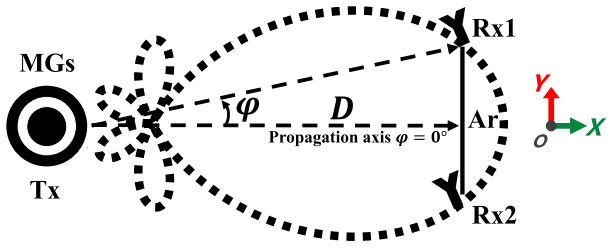

Fig. 3. Typical 2×2 channel model of PSOAM MG multiplexing link using the PASR scheme. TX/Rx: the transmitting and receiving antennas; D: the communication distance; Ar: the receiving aperture; φ: the azimuthal angle at the transverse plane.

Furthermore, what is noteworthy is that the MG still possesses the spiral phase distribution [13] in the azimuthal direction similar to the conventional OAM wave. Without special beam optimization methods, it is hard for common phased array antennas [24] to achieve the same goal. Hence, it can be considered that the MG also has vorticity. As can be seen from the power of the red term in (2), the vorticity is related to l_0^n, Δl and M. The phase slope within its mainlobe can be defined as the equivalent OAM order l_e^n of MG^n, and its value can be described as

$$l_e^n = l_0^n + \Delta l \cdot (\frac{M-1}{2}). \tag{3}$$

Due to similar helical phase distribution, with the help of the PASR scheme [22], the data streams carried by multiple MGs can be demultiplexed orthogonally with a lower receiver complexity. The typical channel model diagram of PSOAM MG multiplexing link using the PASR scheme is shown in Fig. 3; to make it easier to be understood, the model is illustrated as a 2×2 communication link. To use the PASR scheme, hereinafter conditions need to be met: i)

1) multiple MGs need to be radiated coaxially;
2) the number of the receiving antennas must be at least equal to the number of multiple MGs; and
3) the receiving antennas need to be placed uniformly within MG's mainlobe along the azimuthal direction. For the special situation of a 2×2 communication link, as shown in Fig. 3, the receiving antennas need to be placed symmetrically along the propagation axis.

Considering any two high-gain pencil beams realized by PSOAM MGs with the equivalent OAM order l_e^1 and l_e^2, respectively,

$$F_{\mathrm{MG}^1}(\varphi) = \frac{\sin(\frac{M_1\varphi}{2})}{\sin(\frac{\varphi}{2})} \cdot e^{jl_e^1\varphi} \tag{4}$$

$$F_{\mathrm{MG}^2}(\varphi) = \frac{\sin(\frac{M_2\varphi}{2})}{\sin(\frac{\varphi}{2})} \cdot e^{jl_e^2\varphi} \tag{5}$$

Under the PASR scheme [22], for $2\pi/\xi$ azimuthal arc within the mainlobe and Q receiving antennas, the angle difference between adjacent antennas meets $2\pi/(\xi Q)$. If the difference value of equivalent OAM order $\Delta l_e^{12} = l_e^1 - l_e^2$ is equal to $k\xi$, where k is a nonzero integer, the two sampled MG^1 and MG^2

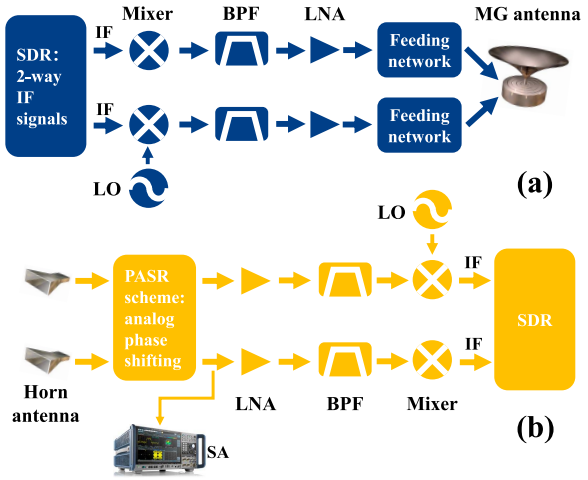

Fig. 4. Schematic of the 2×2 PSOAM MG multiplexing link usifn the PASR scheme: (a) transmitting end and (b) receiving end. SDR: software-defined radio platform; IF: intermediate frequency signal; LO: local oscillator; BPF: bandpass filter; LNA: low-noise amplifier; SA: spectrum analyzer, R&SFSW67.

can still remain the orthogonality between each other

$$\begin{aligned}
&\sum_{q=1}^{Q} F_{\mathrm{MG}^1} \cdot F_{\mathrm{MG}^2}^* \\
&= \sum_{q=1}^{Q} \frac{\sin(\frac{M_1 2\pi q/\xi Q}{2})}{\sin(\frac{2\pi q/\xi Q}{2})} \cdot \frac{\sin(\frac{M_2 2\pi q/\xi Q}{2})}{\sin(\frac{2\pi q/\xi Q}{2})} \cdot e^{jl_e^1 \frac{2\pi q}{\xi Q}} \cdot e^{-jl_e^2 \frac{2\pi q}{\xi Q}} \\
&= \eta \sum_{q=1}^{Q} e^{j \cdot \frac{l_e^1 - l_e^2}{\xi} \cdot \frac{2\pi q}{Q}} \\
&= 0 \\
&s.t. \quad Q \geq 2, \ k \in \mathbb{Z} \cap k \neq 0, \ l_e^1 - l_e^2 = k\xi
\end{aligned} \tag{6}$$

where η contains all the constants; by this time, the sampled power of receiving antennas is the same, the amplitude factors of MGs can be moved out of the summation sign, and theoretically, the MGs are orthogonal strictly. Even though the sampled power of receiving antennas is not equal completely, if their values do not differ much, (6) will still be close to 0. Under this circumstance, two multiplexed MGs can still be considered nearly orthogonal. In practice, the latter situation will be more common. The orthogonality will be impacted mainly by the phase linearity within MG's mainlobe and the accuracy of receiving antennas' placements according to (6). In addition, deterioration of orthogonality is primarily reflected in the decrease in channel isolation [2].

As can be seen from (6), the angle difference in adjacent receiving antennas in azimuthal direction will be constrained by Δl_e between multiplexed MGs, i.e., the PASR scheme needs a specific receiving aperture A_r. For the case of two MGs multiplexing, the specific A_r can be given by [21]

$$A_r = 2 - D \cdot \tan(\varphi_a/2) = 2 - D \cdot \tan(\pi/2\Delta l_e) \tag{7}$$

where φ_a refers to the angle difference in the azimuthal direction between the neighboring receiving antennas.

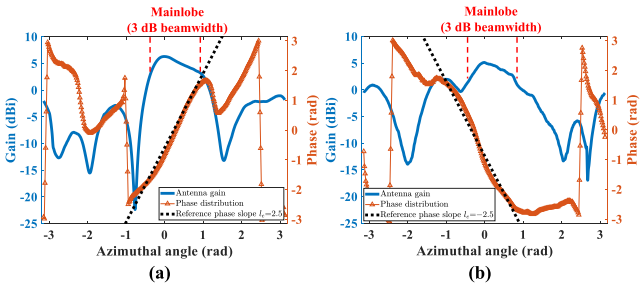

Fig. 5. Measured far-field directivity and phase distribution for (a) $\mathrm{MG}^1\{1, 2, 3, 4\}$ and (b) $\mathrm{MG}^2\{-1, -2, -3, -4\}$ at the XOY plane ($\theta = 90°$).

B. System Architecture

Fig. 4 shows the block diagrams of the 2×2 PSOAM MG multiplexing communication link using the PASR scheme. For the transmitting end shown in Fig. 4(a), using the OFDM technique [25], two modulated baseband signals with a 20 MHz bandwidth whose intermediate frequency (IF) is 800 MHz can be generated by a software-defined radio (SDR, YunSDR Y410s) platform. Two 9.36 GHz continuous wave (CW) signals (local oscillator, LO) are fed to the LO ports of the corresponding mixers, and two IF signals are fed to the IF ports; at this point, the baseband signals will be upconverted to the carrier frequency f_c of 10.16 GHz (RF signals). Passing through the bandpass filters (BPFs) first and low-noise amplifiers (LNA) then, two RF signals carrying different data streams are going to be input to the amplitude–phase adjustable feeding networks [16]. Each feeding network is made up of four electrically adjustable phase shifters, four electrically adjustable attenuators, and a power divider, which can be used for manipulating the intensity and the initial phase of each PSOAM wave among an MG. By virtue of the mentioned feeding networks and the MG antenna, two MGs can be radiated into free space.

The PSOAM MG antenna [16] consists of several coaxial resonators and a reflector. The photograph of the fabricated antenna is shown in Fig. 6(a). Such antenna can generate eight PSOAM modes simultaneously and its total physical aperture is merely 17 cm. All eight PSOAM modes can be controlled independently by the above-mentioned feeding network and divided into multiple MGs as needed. Fig. 5(a) and (b) shows the measured far-field directivity and phase distribution of $\mathrm{MG}^1\{1, 2, 3, 4\}$ and $\mathrm{MG}^2\{-1, -2, -3, -4\}$ at XOY plane, respectively. The mainlobe magnitude and 3 dB beamwidth of the azimuthal angle for MG^1 and MG^2 are 6.3 dBi, 71° and 5.1 dBi, 66°, respectively. Moreover, the measured phase within two MGs' mainlobes possesses the linear distribution with respect to the azimuthal angle, which verifies that an MG has the directionality and vorticity. Besides, the linearity of phase slope is about good, and the measured values are in good agreement with the corresponding reference values. The estimated values of l_e^1 and l_e^2 are 2.5 and -2.5, respectively, which means that these two MGs have orthogonality under the PASR scheme. Due to the machining errors and the generation of standing wave components in resonators, the intensity patterns of two MGs are not exactly the same as they should be. For MG^2, the level of its first sidelobe is a little higher,

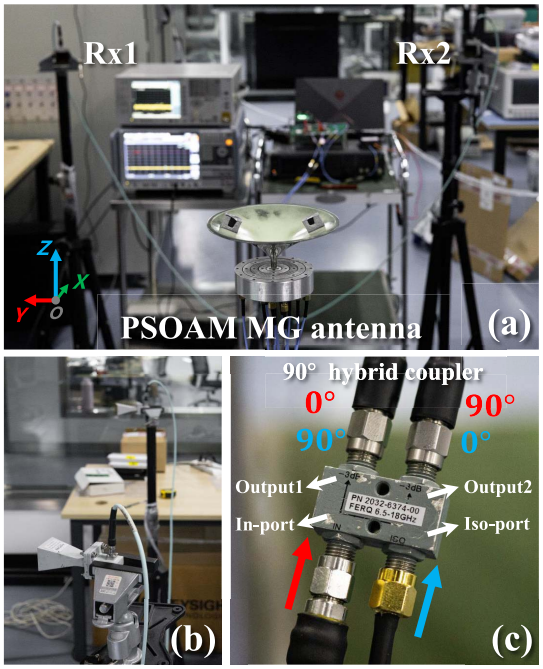

Fig. 6. (a) Experimental setup of the communication link. (b) Receiving end adopts the standard gain horn antennas, and they are placed symmetrically on both sides of the propagation axis. (c) 90° hybrid coupler can be used for demultiplexing the signals based on the PASR scheme.

which leads to a slight decrease in beam gain. This issue might have impact on the orthogonality, which will be reflected in the decrease in channel isolation. Hence, in Section III, the channel isolation caused by MG's orthogonality should be evaluated before carrying out the multiplexing communication experiment. In addition, the design parameters and other performances of this antenna have been taken on and discussed meticulously in preceding works [16], [21].

As shown in Fig. 4(b), after the transmission in a realistic LoS environment, the RF signals arrive at the receiving antennas. Then, the signals will be input into the PASR demultiplexing module, and the demultiplexing process can be totally realized by analog phase shifting method with a very low receiver complexity rather than software implementation like MIMO systems do. Before importing into LNAs, the RF signals can also be input to the spectrum analyzer (SA, Rohde&Schwarz FSW67) to analyze their characteristics in the frequency domain, in which the channel isolation can be measured for evaluating the orthogonality. The RF signals will pass through the corresponding LNAs and BPFs next. Following by getting through the mixers, the RF signals will be downconverted to the IF signals at 800 MHz. Ulteriorly, the IF signals are fed to the SDR platform to achieve the process of signal demodulation. Finally, the baseband signals can be recovered, and their BER performances and received constellation diagrams with corresponding error vector magnitude (EVM) can be calculated and analyzed in the upper computer.

III. Experimental Results

Fig. 6(a) shows the experimental setup of the communication link in an LoS scenario. The total number M of PSOAM

modes in each MG must be the same and the mode interval Δl must be set as 1, which can make sure that the directionality of each MG can stay almost consistent [13]. According to that, a pair of MGs used for conducting the experiments are $MG^1\{1, 2, 3, 4\}$ with l_e^1 of 2.5 and $MG^2\{-1, -2, -3, -4\}$ with l_e^2 of -2.5, and their difference value of equivalent OAM order Δl_e^{12} is equal to 5. The communication distance is set as 2 m. On the basis of (7), φ_a can be calculated as 36°, so A_r needs to be set as 1.29 m. According to Fig. 5, both the receiving antennas are located in the mainlobes of these two MGs, which guarantees that two signals with different vorticity can be sampled.

The receiving end adopts standard gain horn antennas to form the uniform linear array, which guarantees that they could be placed symmetrically along the propagation axis as shown in Fig. 6(b). Based on the PASR scheme [22], for the case of two MGs multiplexing, a group of phase shift should be set as 0° at Rx1 and 90° at Rx2 to demultiplex MG^1. At the same time, the other group of phase shift should be set as 90° at Rx1 and 0° at Rx2 to demultiplex the other one. In our experiments, a 90° hybrid coupler [26] is used for realizing such analog phase shift operation simultaneously, as shown in Fig. 6(c). When in-port is excited, the signal is divided into two parts: the half-power in-phase signal from output port 1 and the half-power signal with 90° phase shift from output port 2. Similarly, when isolation port is excited, the signal is still divided into two parts: the half-power signal with 90° phase shift from output port 1 and the half-power in-phase signal from output port 2. It is worth noting that the aforesaid functionality can also be implemented by several power dividers and phase shifters.

A. Isolation Between Multiplexed MGs

Before carrying out wireless transmission experiments, the channel isolation [2] between multiplexed MGs under the PASR scheme should be evaluated. Considering that the baseband signals transmitted in the existing communication system [27] mostly have a certain bandwidth to achieve higher communication capacity [28], it is necessary to verify the isolation feature over the entire working band. We measured it using not only the single-tone signal but also the bandpass signal. To the best of our knowledge, it is rare to use the bandpass signal to test it in most of the OAM-based communication systems [1]–[3], [11], [29].

As for the single-tone signal test, at the transmitting end, a 10.162 GHz CW signal and a 10.161 GHz CW signal are fed to MG^1 and MG^2, respectively, where their power is consistent. At the receiving end, by virtue of the PASR scheme, a power transfer matrix can be obtained using SA. Then, the isolation between multiplexed MGs can be calculated by such a matrix. During the testing process, the resolution bandwidth (RBW) and the video bandwidth (VBW) of the SA are set as 10 kHz and 30 Hz, respectively.

Fig. 7 shows the result of no phase shifting operation, i.e., the PASR scheme is not used. Two CW signals are at almost the same power level, and their values are -45.74 and -46.10 dBm, respectively. Using the PASR scheme, Fig. 8(a)

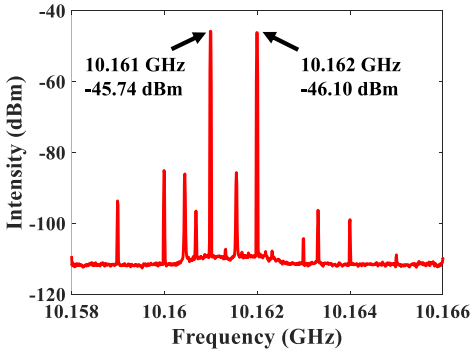

Fig. 7. Single-tone signal test: the result of no demultiplexing operation. The RBW is set as 10 kHz, and the VBW is set as 30 Hz.

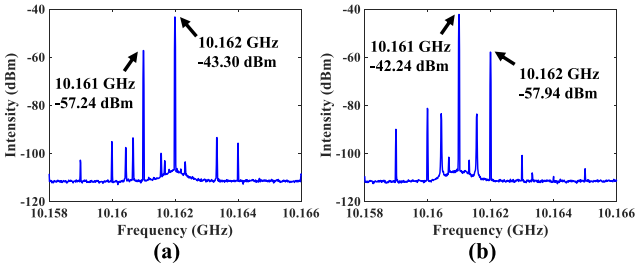

Fig. 8. Using the PASR scheme to (a) demultiplex MG^1 carrying 10.162 GHz CW signal and (b) demultiplex MG^2 carrying 10.161 GHz CW signal. Likewise, the RBW is set as 10 kHz, and the VBW is set as 30 Hz.

shows the demultiplexing of MG^1 carrying 10.162 GHz CW signal, the measured intensity is -43.30 dBm, and this value is increased by 2.8 dB compared with that of no demultiplexing, while the intensity of MG^2 drops to -57.24 dBm. In the same way, Fig. 8(b) shows the demultiplexing of MG^2 carrying 10.161 GHz CW signal, the measured intensity is -42.24 dBm, and this value is increased by 3.5 dB compared with that of no demultiplexing, while the intensity of MG^1 has been suppressed to -57.94 dBm. So far, the power transfer matrix can be obtained, as given in Table I. It can be seen that the channel isolation between two MGs under the PASR scheme is about 15 dB, which means that multiplexed MGs are orthogonal to each other to a certain extent. The isolation performance would be mainly impacted by the following practical factors: the imperfect PSOAM MGs' generation, the inconsistency of link insert loss, and the misalignment between the transmitting/receiving antennas.

As for the bandpass signal test, first, at the transmitting end, a 20 MHz bandpass signal is merely fed to MG^1, while the port of MG^2 is disabled. The modulation formats are QPSK and 16 QAM. The LO power and the gain of the receiving LNA are set as 10 dBm and 45 dB, respectively. At the receiving end, using the PASR scheme, the spectrum of the receiving signals, the BER performance, and the constellations can be measured from both the output ports of the 90° hybrid coupler.

Fig. 9(a) shows the typical receiving spectrums when only the port of MG^1 is enabled, where the power of transmitting IF signal is set as -33 dBm. It can be seen that the central subcarrier of a typical OFDM symbol with a bandwidth of 20 MHz is set to null for overcoming the issues of

TABLE I

POWER TRANSFER MATRIX OF SINGLE-TONE SIGNALS

Received power (dBm)	Rx: MG^1	Rx: MG^2
Tx: MG^1 10.162 GHz	−43.30	−57.94
Tx: MG^2 10.161 GHz	−57.24	−42.24
Isolation (dB)	**13.94**	**15.7**

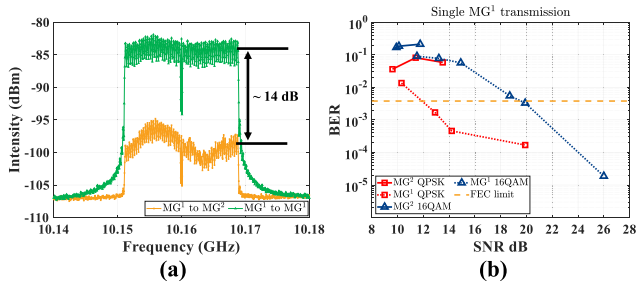

Fig. 9. Using the PASR scheme to demultiplex MG^1 carrying the 20 MHz bandpass signal. (a) When the bandpass signal is merely fed into MG^1 at the transmitting end, and the receiving signal spectrum is measured from both the output ports of the hybrid coupler. The RBW is set as 30 kHz, and the VBW is set as 30 Hz. (b) When QPSK and 16-QAM signals with the 20 MHz bandwidth are merely fed into MG^1, the corresponding raw BER curves of MG^1 channel and MG^2 channel.

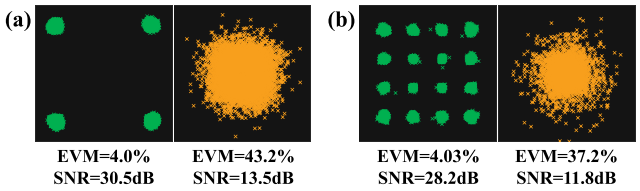

Fig. 10. When (a) QPSK and (b) 16-QAM signals are merely fed into MG^1 at the transmitting end, the measured constellations with EVM performance: MG^1 channel (green) and MG^2 channel (yellow).

dc shifting [30]. Besides, the subcarrier interval is set as 312.5 kHz [31]. The power level of MG^1 channel (green line) is ∼14 dB higher than that of MG^2 channel (yellow line). The measured BER performances are shown in Fig. 9(b). It can be seen that all BER curves of MG^1 channel can reach the forward error correction (FEC) limit of 3.8×10^{-3} [32]. The MG^1 channel can attain the FEC limit at an SNR of 12.9 and 19.9 dB for QPSK and 16 QAM transmission, respectively. In contrast, the BER curves of MG^2 channel cannot reach the FEC limit completely, that is because the SNR will deteriorate rapidly and its value is not enough to be used for signal demodulation [31] owing to the existence of channel isolation. Obviously, in this case, the BER performance of MG^2 channel for both the modulation formats are all above the level 3.62%, and it is an unacceptable level [27].

Furthermore, for QPSK transmission, when the power of transmitting IF signal, the LO power, and the gain of receiving LNA are set as −33 dBm, 10 dBm, and 45 dB, respectively, the attainable SNR of the receiving IF signal for MG^1 channel is 30.5 dB. Conversely, the receiving IF signal's attainable SNR of MG^2 channel is only 13.5 dB. As shown in Fig. 10(a), the EVM of MG^1 channel is 4.0%. For the 16-QAM transmission, the experimental parameters keep the same, the attainable SNR of the receiving IF signal for MG^1 channel is 28.2 dB, while that value of MG^2 channel is only 11.8 dB. As shown in

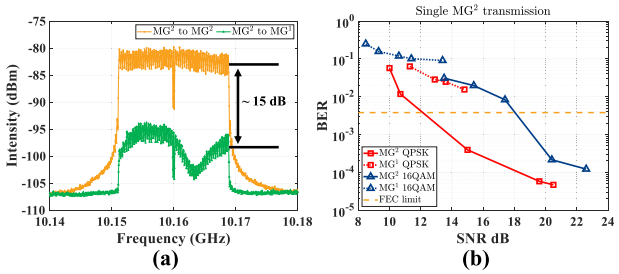

Fig. 11. Using the PASR scheme to demultiplex MG^2 carrying the 20 MHz bandpass signal. (a) When the bandpass signal is merely fed into MG^2, the receiving signal spectrum is measured from both the output ports of the hybrid coupler. The RBW is set as 30 kHz, and the VBW is set as 30 Hz. (b) When the QPSK and 16-QAM signals are merely fed into MG^2, the corresponding raw BER curves of MG^1 channel and MG^2 channel.

Fig. 10(b), the EVM of MG^1 channel is 4.03%. Besides, due to the channel isolation, both the constellations of MG^2 channel are aliasing distinctly.

Similarly, the measurement method and the experimental parameters for evaluating the isolation of MG^2 channel relative to MG^1 channel remain unchanged. At the transmitting end, the port of MG^2 is enabled, while the port of MG^1 is disabled. Fig. 11(a) shows the representative spectrums when the power of transmitting IF signal is set as −33 dBm. As can be seen that the power level of MG^2 channel (yellow line) is ∼15 dB higher than that of MG^1 channel (green line), likewise such the superiority profits from the channel isolation caused by the orthogonality between multiplexed MGs under the PASR scheme. In this case, the measured BER curves are given in Fig. 11(b). The BER curves of MG^2 channel can reach the FEC limit. On the contrary, the BER performances of MG^1 channel could not reach it analogously. In addition, MG^2 channel's BER performances are all more than a BER level of 1.55%, and such a deterioration degree means that the signal cannot be recovered even with the FEC codes.

For the situation of QPSK transmission, when the power of transmitting IF signal, the LO power, and the gain of receiving LNA are set as −33 dBm, 10 dBm, and 45 dB, respectively, the attainable SNR of the receiving IF signal for MG^2 channel is 26 dB. However, the receiving IF signal's attainable SNR of MG^1 channel is merely 13.6 dB. Fig. 12(a) shows that the EVM of MG^2 channel is equal to 2.25%, while the constellation of MG^1 channel is aliasing severely because of channel isolation. For the 16-QAM transmission, the attainable SNR of the receiving IF signal for MG^2 channel is 25.3 dB; meanwhile, that value of MG^1 channel is just 13.4 dB. As shown in Fig. 12(b), the EVM of MG^2 channel is 2.5%. Similarly, the constellation of MG^1 channel is also aliasing.

By reason of foregoing, the channel isolation degree between multiplexed MG^1 and MG^2 under the PASR scheme can maintain the level of about 15 dB for the cases of single-tone signal and bandpass signal. It is adequate for establishing a dual-channel data multiplexing link when the receiving SNR is large enough [2], [3], [33]–[35].

B. Data Multiplexing

At the transmitting end, two QPSK signals carrying different data streams with 20 MHz bandwidth are fed simultaneously

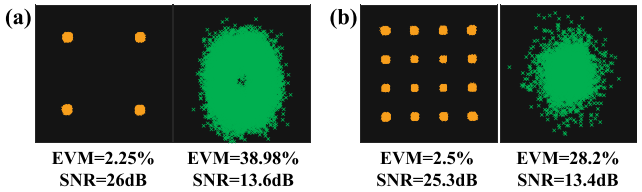

Fig. 12. When (a) QPSK and (b) 16-QAM signals are merely fed into MG^2, the measured constellations with EVM performance: MG^1 channel (green) and MG^2 channel (yellow).

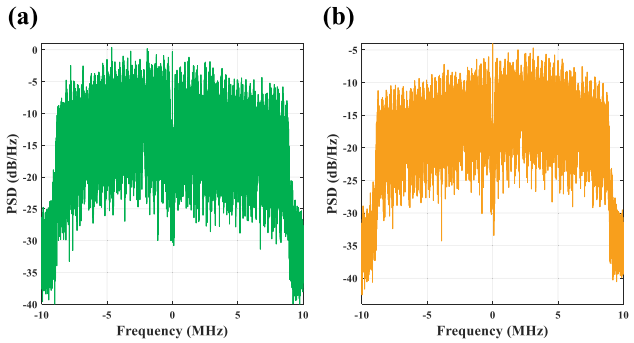

Fig. 13. PSD of the receiving IF signals from (a) MG^1 channel at an SNR of 18.2 dB and (b) MG^2 channel at an SNR of 18.9 dB. The modulation format is QPSK.

to MG^1 and MG^2, respectively. At the receiving end, the analog phase shifting operation based on the PASR scheme can be implemented by pure hardware to demultiplex the MGs orthogonally with a lower complexity.

Let us start off by observing the frequency-domain characteristics of the receiving signals. Fig. 13(a) and (b) shows the power spectral density (PSD) of the receiving IF signals from MG^1 channel at an SNR of 18.2 dB and MG^2 channel at an SNR of 18.9 dB, respectively. The spectrum can be obtained by virtue of fast Fourier transformation (FFT) [36] to do the calculation of the received IF signal in the upper computer, where the IF signal is sampled by the analog-to-digital (ADC) circuit [37] in the SDR platform. Especially, there is the *sag phenomenon* at the zero frequency, which can be regarded as the typical feature of an OFDM symbol [38].

Fig. 14(a) gives the measured BER performances. It can be seen that both the curves are able to reach the FEC limit, which has proved the validity of such communication link. In terms of what we measured, for MG^1 channel, it can attain the FEC limit at a receiving SNR of 13.4 dB. For MG^2 channel, the required receiving SNR is 13.3 dB. Besides, Fig. 14(b) and (c) shows the typical constellations with the measured EVM at the corresponding SNR level. The EVM performances from MG^1 channel are 18.0% and 25.3% at the SNR of 18.2 and 15.1 dB, respectively. Likewise, for MG^2 channel, its EVM values are 18.6% and 24.1% at the SNR of 18.9 and 15.0 dB, respectively. In our system, the OFDM symbol is made up of 56 subcarriers, in which only 52 subcarriers are set to be used for actual data transmission. Therefore, just like most of the existing communication systems using OFDM technique [2], [21], the attainable spectrum efficiency (SE) of the QPSK

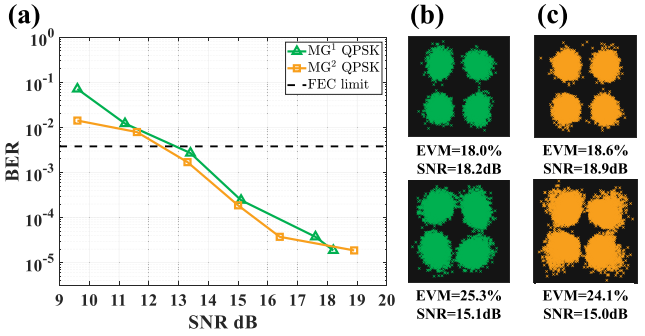

Fig. 14. (a) Measured BER performances of QPSK multiplexing. (b) Typical constellations with EVM performance from MG^1 channel at the corresponding SNR. (c) Typical constellations with EVM performance from MG^2 channel.

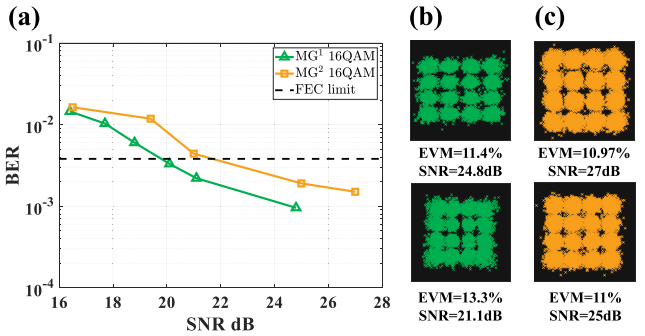

Fig. 15. (a) Measured BER performances of 16-QAM transmission. (b) Measured constellations with EVM performance from MG^1 channel at different SNRs. (c) Measured constellations with EVM performance from MG^2 channel.

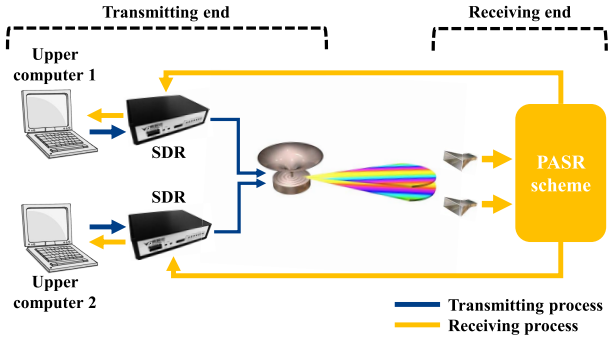

Fig. 16. Signal flow diagram of the real-time dual-channel video transmission link. Two different video signals are carried by MG^1 and MG^2, respectively.

transmission could be calculated as 3.7 bits/s/Hz (2 bits per symbol $\times$ 2 multiplexed MGs $\times$ (52/56)).

To used high-order modulation format for achieving higher SE, the 16-QAM transmission test has been carried out. Similar to the frame structure of QPSK transmission, the attainable SE would be 7.4 bits/s/Hz [4 bits per symbol $\times$ 2 multiplexed MGs $\times$ (52/56)]. As shown in Fig. 15(a), both the BER curves of two channels can still attain the FEC limit. Furthermore, Fig. 15(b) and (c) illustrates the typical constellations with EVM performance at the corresponding SNR level. The measured EVM values from MG^1 channel are 11.4% and 13.3% at the SNR of 24.8 and 21.1 dB, respectively. In addition, for MG^2 channel, its EVM performances

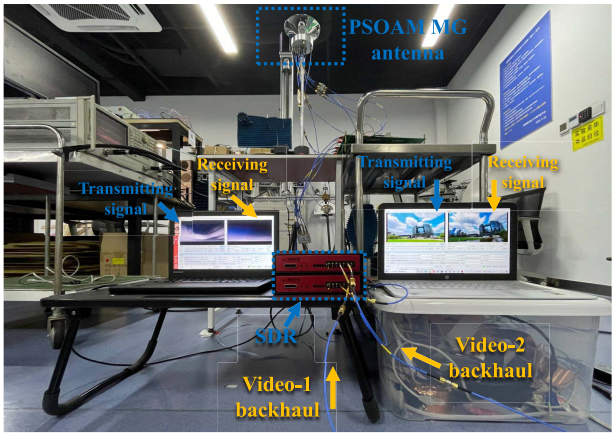

Fig. 17. Experimental photography to demonstrate successful transmission of dual video signals in real-time. The experiment site is located in Yuquan campus of Zhejiang University. The transmitted videos are *The Best of Nanjing* (left) and *Time-portrayed Hangzhou* (right), respectively; the copyrights belong to the original authors.

are 10.97% and 11% at the SNR of 27 and 25 dB, respectively. For higher modulation formats, such as 64 QAM, it has been verified that the existing channel isolation cannot support its transmission after our tests.

C. Real-Time Video Transmission

Moreover, we attempt to build a dual-channel video transmission link in an LoS scenario to display signal demultiplexing visually in real-time. Fig. 16 shows the signal flow diagram of such link. The demonstration system adopts the loopback way, which is the routing of data streams back to their source for signal processing. In addition, the proposed system is set up based on the IEEE 802.11a standard [39], [40].

At the transmitting end, two different digital video signals are transmitted to the SDR platforms by the upper computers and then converted into the analog IF signals in the SDR platforms. Getting through the mixers, such signals can be upconverted to carrier frequency and then fed into MG^1 and MG^2, respectively. At the receiving end, the video signals are demultiplexed using the PASR scheme, after passing through the mixers, and the receiving IF signals can be obtained and then transmitted back to the SDR platforms at the transmitting end. Finally, the video signals can be demodulated and displayed on the corresponding upper computers in real-time. In the above section, it has been proven that the existing channel isolation is sufficient to support 16-QAM transmission. Hence, both the video signals adopt the 24 Mbps 16 QAM 1/2 coding rate format according to the 802.11a protocol [39].

Fig. 17 shows the experimental scenario, and real-time dual-channel video transmission has been carried out successfully. When conducting such an experiment, there is a certain delay in video transmission; however, both the videos can play smoothly, which verifies the orthogonality between multiplexed MGs more intuitively. The above-mentioned results show that two separate wireless channels with the certain isolation are established successfully based on the PSOAM MG antenna under the PASR scheme. Furthermore, when the PASR scheme is not enabled properly, two video signals will

Fig. 18. Without the phase shifting operation based on the PASR scheme, the channel isolation will cease to exist, and the multiplexed video signals are going to be aliased.

be aliased due to the disappearance of isolation. As shown in Fig. 18, the received videos all occur with the *Mosaic* problem, which suffers from that the digital video signals cannot be decoded correctly.

IV. Discussion

The comparison of the proposed work with other analog spatial multiplexing transmission systems is shown in Table II. The so-called "analog" means that the demultiplexing process is implemented by pure hardware rather than algorithm. Moreover, there are several points that need to be explained further. The bandwidth in [1] is not given directly, such value in Table II is calculated based on data rates and total SE. The remaining performance parameters can be obtained firsthand from relevant references. In [2], only the QPSK signal transmission experiment uses the analog demultiplexing method, and other experiments adopt sparse channel equalization. In [41], a novel OAM-based direct antenna modulation (DAM) [42] system has been demonstrated. In this system, a digital symbol is mapped to a particular OAM mode and transmitted to the receiving end directly. The implementation method of communication link in [43] adopts the radio-over-fiber (RoF) technique; besides, other works all adopt the RF link.

For the analog demultiplexing method, the channel isolation is affected by communication distance. All the systems in Table II are merely suitable for short-range point-to-point wireless communication. In [2], the cassegrain antenna with double reflectors is used for converging OAM waves, and its link achieves the longest distance of 10 m.

In terms of system complexity, the OAM-based DAM system [41] possesses significant superiority. Due to that, it can remove some active devices such as mixers, power amplifiers, and related auxiliary circuits, and such an architecture may have superiorities in low complexity and low power consumption. Its data rate performance depends on the switching speed of beam pattern. Shuang *et al.* [41] claimed that the 100 MHz switching speed can be achieved.

In Table II, highest data rate and highest total SE are 32 Gbits/s and 16 bits/s/Hz [1], respectively, and such link uses four OAM modes, two polarizations, and 16-QAM modulation format. However, its bandwidth performance is not optimal. The data rate mainly depends on the SE and the

TABLE II
COMPARISON WITH OTHER WORKS

Ref.	Implementation method	A_t / A_r (m)	Carrier frequency (GHz)	Distance (m)	Measured channel isolation (dB)	Modulation	Single-way SE (bits/s/Hz/stream)	Number of multiplexing	Total SE (bits/s/Hz)	Bandwidth/ relative bandwidth	Data rate
[1]: OAM+Polaization	RF	0.3 / 0.3	28	2.5	~ 16	16-QAM	2	8	16	2 GHz / 7.14%	32 Gbits/s
[2]: OAM	RF	0.6 / 0.6	10	10	~ 10	QPSK	1.875	4	7.5	40 MHz / 0.4%	300 Mbits/s
[29]: OAM	RF	0.1 / 0.2	60	1.4	~ 20	NA	NA	2	NA	1.75 GHz / 2.9%	NA
[41]: OAM	RF	1.02 / 1.02	3.2	2	NA	DAM	NA	13	NA	Single frequency	100 MBaud/s
[43]: ROM	RoF	0.092 / 0.092	61.5	0.4	~ 13	OOK	0.5	2	1	9 GHz / 14.6%	9 Gbits/s
This work	RF	0.17 / 1.29	10.16	2	~ 15	16-QAM	3.7	2	7.4	20 MHz / 0.2%	148 Mbits/s

bandwidth. The former is related to the modulation format and the number of multiplexing, while the latter relies on the antenna bandwidth and the signal bandwidth generated by the communication module. Thanks to higher antenna bandwidth and bandwidth superiority of RoF link, the rectangular coordinate orthogonal multiplexing (ROM) link [43] realizes largest relative bandwidth of 14.6%. Besides, it also realizes a 9 Gbits/s data rate, and hence, the ROM technique is most likely to be extended to the THz band.

In the aspects of measured channel isolation, single-way SE, and total SE, the performances of our system are relatively good and acceptable. The corresponding performances are $\sim$15 dB, 3.7 bits/s/Hz/stream, and 7.4 bits/s/Hz, respectively. Different from the conventional OAM wave, MG can overcome the phase singularity and severe divergence problems. In general, this article is aimed at verifying the feasibility of PSOAM MG orthogonality multiplexing communication, it can be considered as a proof-of-principle experiment. Hence, there are still some areas for improvement.

Our system mainly possesses two issues: the limited system bandwidth and the relatively large receiving aperture. The former leads to the decrease in data rate. The system bandwidth relies on the antenna bandwidth and the signal bandwidth generated by the communication module. The PSOAM MG antenna in our experiment adopts the resonant structure similar to [2]. Generally, the bandwidth of resonant cavity antennas is narrow, and hence the radiation efficiency and mode purity can be improved. According to [16], such MG antenna's impedance bandwidth is merely 140 MHz. Besides, limited by the performance of our SDR platform, the signal bandwidth is only 20 MHz. To improve the data rate, the future research should be initiated from the following areas. By optimizing the antenna structure, the impedance bandwidth can be increased. Meanwhile, the signal bandwidth also needs to be improved, which requires the update of the communication module. In addition, our proposed system has the scalability in terms of the multiplexing number. We may improve the total SE by increasing the number of data streams or using higher order modulation format, and thus the data rate will be boosted.

Furthermore, the PASR scheme requires a specific receiving aperture which is related to l_e of MG. If without MGs with higher l_e, the proposed system is still a laboratory-level research and cannot become more practical. For such low Δl_e in this article, the PASR scheme needs a large or even unacceptable A_r as D increases. For instance, if D is set as 20 m, the corresponding A_r will be extremely big, which can be regarded as an unreasonable A_r for practical application. It is worth noting that if we can generate two MGs with Δl_e of 205 [44], for the same D, the corresponding A_r can be reduced to $\sim$0.31 m. The biggest difficulty for fabricating this kind of antenna is to find a high-precision machining method of metal cavity. This work is ongoing. To sum up, it is necessary to generate an MG with higher l_e, and the partial arc transmitting (PAT) scheme might be a feasible way to achieve that [45], [46]. In addition, to further improve channel isolation, we should generate PSOAM MGs with more perfect spiral phase distributions, i.e., each PSOAM mode among the MG needs to possess the good mode purity characteristic.

V. CONCLUSION

We have demonstrated a PSOAM MG orthogonal multiplexing communication link at the X-band using the PASR scheme experimentally. The channel isolation between multiplexed MGs has also been evaluated, and it can maintain the level of 15 dB approximately. Furthermore, it has been verified that such an isolation is adequate for building a reliable 16-QAM transmission link with an attainable SE of 7.4 bits/s/Hz in a realistic LoS environment. Finally, by virtue of the proposed communication architecture, a real-time dual-channel video transmission experiment has been conducted successfully to prove the orthogonality between multiplexed MGs under the PASR scheme intuitively. Different from [21], the demultiplexing process in this work is realized only by the analog phase shifting operation, where the receiver complexity can be reduced dramatically.

ACKNOWLEDGMENT

Xiaowen Xiong would like to express sincere gratitude to his advisors Prof. S. Zheng and Prof. X. Zhang for the guidance and support. He is also grateful to Y. Chen for assisting him to carry out all experiments in this article.

REFERENCES

[1] Y. Yan *et al.*, "High-capacity millimetre-wave communications with orbital angular momentum multiplexing," *Nature Commun.*, vol. 5, no. 1, pp. 1–9, Sep. 2014.

[2] W. Zhang *et al.*, "Mode division multiplexing communication using microwave orbital angular momentum: An experimental study," *IEEE Trans. Wireless Commun.*, vol. 16, no. 2, pp. 1308–1318, Feb. 2016.

[3] X. Su *et al.*, "Demonstration of 8-channel 32-Gbit/s QPSK wireless communications at 0.28–0.33 THz using 2 frequency, 2 polarization, and 2 mode multiplexing," in *Proc. Opt. Fiber Commun. Conf. (OFC)*, 2021, pp. 1–3.

[4] J. Wang *et al.*, "N-dimentional multiplexing link with 1.036-Pbit/s transmission capacity and 112.6-bit/s/Hz spectral efficiency using OFDM-8QAM signals over 368 WDM pol-muxed 26 OAM modes," in *Proc. Eur. Conf. Opt. Commun. (ECOC)*, Sep. 2014, pp. 1–3.

[5] J. Zheng, S. Zheng, Z. Shao, and X. Zhang, "Analysis of rotational Doppler effect based on radio waves carrying orbital angular momentum," *J. Appl. Phys.*, vol. 124, no. 16, Oct. 2018, Art. no. 164907.

[6] Y. Chen, S. Zheng, X. Jin, H. Chi, and X. Zhang, "Single-frequency computational imaging using OAM-carrying electromagnetic wave," *J. Appl. Phys.*, vol. 121, no. 18, May 2017, Art. no. 184506.

[7] I. B. Djordjevic, "OAM-based hybrid free-space optical-terahertz multidimensional coded modulation and physical-layer security," *IEEE Photon. J.*, vol. 9, no. 4, pp. 1–12, Aug. 2017.

[8] X. Sun and I. B. Djordjevic, "Physical-layer security in orbital angular momentum multiplexing free-space optical communications," *IEEE Photon. J.*, vol. 8, no. 1, pp. 1–10, Feb. 2016.

[9] S. M. Mohammadi *et al.*, "Orbital angular momentum in radio: A system study," *IEEE Trans. Antennas Propag.*, vol. 58, no. 2, pp. 565–572, Feb. 2009.

[10] F. Tamburini, E. Mari, A. Sponselli, B. Thidé, A. Bianchini, and F. Romanato, "Encoding many channels on the same frequency through radio vorticity: First experimental test," *New J. Phys.*, vol. 14, no. 3, Mar. 2012, Art. no. 033001.

[11] Y. Yagi *et al.*, "Field experiment of 117 Gbit/s wireless transmission using OAM multiplexing at a distance of 200 m on 40 GHz band," in *Proc. IEEE Int. Conf. Commun. Workshops (ICC Workshops)*, Jun. 2021, pp. 1–5.

[12] L. Allen, M. W. Beijersbergen, R. J. C. Spreeuw, and J. P. Woerdman, "Orbital angular momentum of light and the transformation of Laguerre–Gaussian laser modes," *Phys. Rev. A, Gen. Phys.*, vol. 45, no. 11, p. 8185, Jun. 1992.

[13] S. Zheng *et al.*, "Realization of beam steering based on plane spiral orbital angular momentum wave," *IEEE Trans. Antennas Propag.*, vol. 66, no. 3, pp. 1352–1358, Mar. 2017.

[14] Z. Zhu *et al.*, "A compact pattern reconfiguration antenna based on multimode plane spiral OAM," *IEEE Trans. Antennas Propag.*, vol. 69, no. 2, pp. 1168–1172, Feb. 2020.

[15] X. Xiong, S. Zheng, Z. Zhu, X. Yu, X. Jin, and X. Zhang, "Performance analysis of plane spiral OAM mode-group based MIMO system," *IEEE Commun. Lett.*, vol. 24, no. 7, pp. 1414–1418, Jul. 2020.

[16] M. J. Padgett, F. M. Miatto, M. P. Lavery, A. Zeilinger, and R. W. Boyd, "Divergence of an orbital-angular-momentum-carrying beam upon propagation," *New J. Phys.*, vol. 17, no. 2, 2015, Art. no. 023011.

[17] C. Craeye, "On the transmittance between OAM antennas," *IEEE Trans. Antennas Propag.*, vol. 64, no. 1, pp. 336–339, Jan. 2015.

[18] J. Xu, "Degrees of freedom of OAM-based line-of-sight radio systems," *IEEE Trans. Antennas Propag.*, vol. 65, no. 4, pp. 1996–2008, Apr. 2017.

[19] K. Murata, N. Honma, K. Nishimori, N. Michishita, and H. Morishita, "Analog eigenmode transmission for short-range MIMO based on orbital angular momentum," *IEEE Trans. Antennas Propag.*, vol. 65, no. 12, pp. 6687–6702, Dec. 2017.

[20] Z. Zhang, S. Zheng, X. Jin, H. Chi, and X. Zhang, "Generation of plane spiral OAM waves using traveling-wave circular slot antenna," *IEEE Antennas Wireless Propag. Lett.*, vol. 16, pp. 8–11, 2016.

[21] X. Xiong *et al.*, "Experimental study of plane spiral OAM mode-group based MIMO communications," *IEEE Trans. Antennas Propag.*, vol. 70, no. 1, pp. 641–653, Jan. 2022.

[22] W. Zhang, S. Zheng, Y. Chen, X. Jin, H. Chi, and X. Zhang, "Orbital angular momentum-based communications with partial arc sampling receiving," *IEEE Commun. Lett.*, vol. 20, no. 7, pp. 1381–1384, Jul. 2016.

[23] B. Jack, M. Padgett, and S. Franke-Arnold, "Angular diffraction," *New J. Phys.*, vol. 10, no. 10, 2008, Art. no. 103013.

[24] R. C. Hansen, *Phased Array Antennas*, vol. 213. Hoboken, NJ, USA: Wiley, 2009.

[25] L. Cimini, Jr., "Analysis and simulation of a digital mobile channel using orthogonal frequency division multiplexing," *IEEE Trans. Commun.*, vol. C-33, no. 7, pp. 665–675, Jul. 1985.

[26] L. Chiu and Q. Xue, "Investigation of a wideband 90° hybrid coupler with an arbitrary coupling level," *IEEE Trans. Microw. Theory Techn.*, vol. 58, no. 4, pp. 1022–1029, Mar. 2010.

[27] A. Goldsmith, *Wireless Communications*. Cambridge, U.K.: Cambridge Univ. Press, 2005.

[28] C. E. Shannon, "Communication in the presence of noise," *Proc. IRE*, vol. 37, no. 1, pp. 10–21, Feb. 1949.

[29] X. Hui *et al.*, "Multiplexed millimeter wave communication with dual orbital angular momentum (OAM) mode antennas," *Sci. Rep.*, vol. 5, no. 1, pp. 1–9, Sep. 2015.

[30] J. Zhao *et al.*, "Programmable time-domain digital-coding metasurface for non-linear harmonic manipulation and new wireless communication systems," *Nat. Sci. Rev.*, vol. 6, no. 2, pp. 231–238, Nov. 2019.

[31] B. O'Hara and A. Petrick, "IEEE 802.11n higher data rates beyond 54 Mbit/s," in *IEEE 802.11 Handbook: A Designer's Companion*. New York, NY, USA: Wiley, 2005, pp. 327–331.

[32] E. A. Lee and D. G. Messerschmitt, *Digital Communication*. Norwell, MA, USA: Springer, 2012.

[33] F. Tamburini *et al.*, "Tripling the capacity of a point-to-point radio link by using electromagnetic vortices," *Radio Sci.*, vol. 50, no. 6, pp. 501–508, 2015.

[34] H. Y. Chung and S. G. Wilson, "Multimode modulation and coding of QAM," *IEEE Trans. Commun.*, vol. 41, no. 1, pp. 1–6, Jan. 1993.

[35] W. T. Webb and L. Hanzo, *Modern Quadrature Amplitude Modulation: Principles and Applications for Fixed and Wireless Channels: One*. Hoboken, NJ, USA: Wiley, 1994.

[36] S. K. Mitra and Y. Kuo, *Digital Signal Processing: A Computer-Based Approach*, vol. 2. New York, NY, USA: McGraw-Hill, 2006.

[37] R. J. Van de Plassche, *CMOS Integrated Analog-to-Digital and Digital-to-Analog Converters*, vol. 742. New York, NY, USA: Springer, 2013.

[38] Y. S. Cho, J. Kim, W. Y. Yang, and C. G. Kang, *MIMO-OFDM Wireless Communications With MATLAB*. Hoboken, NJ, USA: Wiley, 2010.

[39] *IEEE Standard for Information Technology—Local and Metropolitan Area Networks—Specific Requirements—Part 11: Wireless LAN Medium Access Control (MAC) and Physical Layer (PHY) Specifications: Further Higher Data Rate Extension in the 2.4 GHz Band*, IEEE Standard 802.11g-2003 (Amendment to IEEE Standard 802.11, 1999 Edn. (Reaff 2003) as amended by IEEE Standard 802.11a-1999, 802.11b-1999, 802.11b-1999/Cor 1-2001, and 802.11d-2001), 2003, pp. 1–104.

[40] B. Zhang, Z. Gao, F. Gao, and D. Hsu, "Performance of video over an IEEE 802.11a wireless LAN," in *Proc. Int. Conf. Mech. Sci., Electric Eng. Comput. (MEC)*, Aug. 2011, pp. 2127–2130.

[41] Y. Shuang, H. Zhao, W. Ji, T. J. Cui, and L. Li, "Programmable high-order OAM-carrying beams for direct-modulation wireless communications," *IEEE J. Emerg. Sel. Topics Circuits Syst.*, vol. 10, no. 1, pp. 29–37, Mar. 2020.

[42] H. Shi and A. Tennant, "Simultaneous, multichannel, spatially directive data transmission using direct antenna modulation," *IEEE Trans. Antennas Propag.*, vol. 62, no. 1, pp. 403–410, Jan. 2013.

[43] T. Tomura, J. Hirokawa, M. Ali, and G. Carpintero, "Millimeter-wave multiplexed wideband wireless link using rectangular-coordinate orthogonal multiplexing (ROM) antennas," *J. Lightw. Technol.*, vol. 39, no. 24, pp. 7821–7830, Dec. 15, 2021.

[44] Z. Zhu, X. Xiong, Y. Chen, S. Zheng, and X. Zhang, "A fan ring resonator antenna for generating high gain PSOAM mode-group with ultrahigh equivalent order," in *Proc. IEEE Int. Conf. Commun. Workshops (ICC Workshops)*, Jun. 2021, pp. 1–5.

[45] X. Xiong *et al.*, "Direct generation of OAM mode-group and its application in LoS-MIMO system," *IEEE Commun. Lett.*, vol. 24, no. 11, pp. 2628–2631, Nov. 2020.

[46] Z. Zhu *et al.*, "A non-uniform travelling-wave current source model for designing OAM antenna: Theory, analysis and application," *IEEE Access*, vol. 10, pp. 47499–47508, 2022.

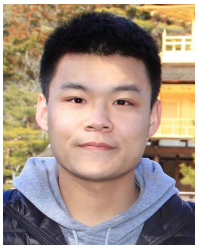

Xiaowen Xiong (Member, IEEE) received the B.S. degree in communication engineering from the Nanjing University of Posts and Telecommunications, Nanjing, China, in 2017, and the Ph.D. degree in electronic science and technology from Zhejiang University, Hangzhou, China, in 2022.

His current research interests include RF and microwave systems, wireless communication, OAM wave, and its applications.

Dr. Xiong was a recipient of the Best Student Paper Honorable Mention at the 2021 IEEE MTT-S International Wireless Symposium (IWS2021), Nanjing, China. He served as the Reviewer for IEEE COMMUNICATIONS LETTERS and IEEE WIRELESS COMMUNICATIONS LETTERS.

Shilie Zheng (Member, IEEE) received the B.S. and M.S. degrees in materials science and the Ph.D. degree in physical electronics and optoelectronics from Zhejiang University, Hangzhou, China, in 1995, 1998, and 2003, respectively.

In 1998, she joined the Department of Information Science and Electronic Engineering, Zhejiang University, where she was appointed as an Associate Professor in 2005. From November 2005 to March 2006, she spent five months with Tohoku University, Sendai, Japan, as a Research Assistant. From July 2016 to July 2017, she was a Visiting Research Fellow with the RF and microwave Laboratory, National University of Singapore, Singapore. In 2017, she was appointed as a Full Professor with Zhejiang University. Her current research interests include twisted radio waves and applications, microwave photonics, and wireless communications.

Yuqi Chen (Graduate Student Member, IEEE) received the B.S. degree from the University of Electronic Science and Technology of China, Chengdu, China, in 2019. He is currently pursuing the Ph.D. degree in electronic science and technology with Zhejiang University, Hangzhou, China.

His research interests include orbital angular momentum antenna and its applications in wireless communication.

Zelin Zhu (Graduate Student Member, IEEE) received the B.S. degree in electronic information science and technology from the University of Electronic Science and Technology of China, Chengdu, China, in 2018. He is currently pursuing the Ph.D. degree in electronic science and technology with Zhejiang University, Hangzhou, China.

His research interests include vortex electromagnetic wave antenna and its applications in radar system and communication systems.

Xiaonan Hui (Member, IEEE) received the B.S. degree from Northeastern University, Shenyang, China, in 2012, the M.S. degree from Zhejiang University, Hangzhou, China, in 2015, and the Ph.D. degree from Cornell University, Ithaca, NY, USA, in 2021, all in electrical engineering.

In 2021, he joined the College of Information Science and Electronic Engineering, Zhejiang University, as an Assistant Professor. His research interests include wireless sensing, RFID, IoT, and wireless communication systems.

Xianbin Yu (Senior Member, IEEE) is currently a Professor with Zhejiang University, Hangzhou, China. He has given 40+ invited talks in prestigious international conferences within the area of optical communications and RF photonics technologies. He has coauthored three book chapters and 200+ peer-reviewed international journals and conference papers. His research interests are in the areas of ultrafast millimeter-wave/THz photonic information processing, ultrahigh-frequency photonic wireless communication systems, and emerging new applications of millimeter-wave/THz technologies.

Prof. Yu served as a session chair/TPC member for a number of international conferences.

Xiaofeng Jin (Member, IEEE) received the B.S. degree in optical engineering from the Huazhong University of Science and Technology, Wuhan, China, in 1990, the M.S. degree in underwater acousto electronics engineering from the China Ship Building Institute, Beijing, China, in 1993, and the Ph.D. degree in optical engineering from Zhejiang University, Hangzhou, China, in 1996.

In 1999, he was appointed as an Associate Professor with the Department of Information and Electronic Engineering, Zhejiang University, and a Full Professor in 2006. His current research interests include microwave photonics, photonic circuits, components and modules, and smart sensing systems.

Wei E. I. Sha (Senior Member, IEEE) received the B.S. and Ph.D. degrees in electronic engineering from Anhui University, Hefei, China, in 2003 and 2008, respectively.

From July 2008 to July 2017, he was a Post-Doctoral Research Fellow and then a Research Assistant Professor with the Department of Electrical and Electronic Engineering, The University of Hong Kong, Hong Kong. From March 2018 to March 2019, he worked with University College London, London, U.K., as a Marie-Curie Individual Fellow. In October 2017, he joined the College of Information Science and Electronic Engineering, Zhejiang University, Hangzhou, China, where he is currently a tenure-tracked Assistant Professor. He has authored or coauthored 170 refereed journal articles, 140 conference publications (including three keynote talks, one short course, and 36 invited talks), eight book chapters, and two books. His Google Scholar citation is 7400 with an H-index of 43. His research interests include theoretical and computational research in electromagnetics and optics, focusing on the multiphysics and interdisciplinary research. His research involves fundamental and applied aspects in computational and applied electromagnetics, nonlinear and quantum electromagnetics, micro- and nano-optics, optoelectronic device simulation, and multiphysics modeling.

Dr. Sha is a member of Optical Society of America (OSA). In 2015, he was awarded Second Prize of Science and Technology from Anhui Province Government, China. He also received six best student paper prizes and one young scientist award with his students. He served as a reviewer for 60 technical journals and a technical program committee member for ten IEEE conferences. He also served as Associate Editor for IEEE JOURNAL ON MULTISCALE AND MULTIPHYSICS COMPUTATIONAL TECHNIQUES, IEEE OPEN JOURNAL OF ANTENNAS AND PROPAGATION, and IEEE ACCESS.

Xianmin Zhang (Member, IEEE) received the B.S. and Ph.D. degrees in physical electronics and optoelectronics from Zhejiang University, Hangzhou, China, in 1987 and 1992, respectively.

He was appointed as an Associate Professor of information and electronic engineering with Zhejiang University, in 1994, and a Full Professor, in 1999. He was a Research Fellow with the University of Tokyo, Tokyo, Japan, and Hokkaido University, Sapporo, Japan, from November 1996 to September 1997, and October 1997 to September 1998, respectively. In 2007, he spent two months with the Research Laboratory of Electronics, Massachusetts Institute of Technology, Cambridge, MA, USA, as a Visiting Research Fellow. He was the Dean of the Department of Information Science and Electronic Engineering, Zhejiang University, from September 2005 to November 2017, the Dean of the School of Microelectronics, Zhejiang University, from May 2015 to September 2018, the Vice Dean of the Polytechnic Institute, Zhejiang University, from July 2016 to September 2018, the President of the Zhejiang University Ningbo Institute, Ningbo, China, from July 2018 to April 2020, and the Dean of Ningbo Campus, Zhejiang University, from September 2018 to November 2020. He is currently the Vice President of NingboTech University, Ningbo. His research interests include microwave photonics and electromagnetic wave theory and applications.